

physica **p** status **s** solidi **S**

www.pss-journals.com

reprint



Short-wavelength InP quantum cascade laser sources by quasi-phase-matched intracavity second-harmonic generation

Augustinas Vizbaras^{*1}, Matthias Anders¹, Christian Grasse¹, Simeon Katz^{1,2}, Gerhard Boehm¹, Ralf Meyer¹, Mikhail A. Belkin³, and Markus-Christian Amann¹

¹ Walter Schottky Institut, Technische Universität München, Am Coulombwall 3, 85748 Garching, Germany

² Osram Opto-Semiconductors, Leibnitzstr. 4, 93055 Regensburg, Germany

³ Department of Computer and Electrical Engineering, The University of Texas at Austin, 78758 Austin, Texas, USA

Received 22 June 2011, revised 4 August 2011, accepted 10 August 2011

Published online 9 November 2011

Keywords quantum cascade lasers, nonlinear frequency mixing, quasi-phase matching, semiconductor lasers

* Corresponding author: e-mail augustinas.vizbaras@wsi.tum.de, Phone: +49 89 289 12785, Fax: +49 89 289 12704

Short-wavelength quantum cascade laser (QCL) sources, based on transversely integrated giant nonlinearity have been designed and fabricated. Devices consist of an injectorless GaInAs/AlInAs/InP pump QCL and a passive two-well based nonlinearity grown on top of the pump active region. The nonlinearity was designed to possess a giant nonlinear response for the process of second-harmonic generation (SHG). For efficient SHG process,

the wave-vector mismatch between the fundamental and the nonlinear signals was compensated by structuring the nonlinear layer into the 50 % duty-cycle quasi-phase-matching gratings. Using this approach we were able to demonstrate room-temperature operation at 3.5 μm and 2.7 μm second-harmonic emission wavelengths with output power levels up to 30 μW .

© 2011 WILEY-VCH Verlag GmbH & Co. KGaA, Weinheim

1 Introduction Since the first demonstration in 1994, quantum cascade lasers have undergone tremendous improvements. Today, GaInAs/AlInAs/InP based QCLs have turned into reliable, continuous-wave capable laser sources in the 3.8 μm –10 μm wavelength range [1]. However, wavelengths below 3.8 μm are difficult to generate due to limited conduction band offset and increased carrier scattering into the indirect valleys of the well material [2]. An alternative way to generate short-wavelengths is to use materials with large conduction band offsets, such as Sb-based materials [2, 3] or nonlinear frequency conversion. The latter approach is particularly attractive as does not suffer from the carrier leakage into indirect valleys [4] and can in-principle be used for wavelength generation down to at least 2.5 μm with the conventional GaInAs/AlInAs/InP material system.

In this work we describe the design and experimental results of nonlinear devices emitting $\sim 3.5 \mu\text{m}$. Devices successfully operate at room-temperature at threshold current densities as low as 3 kA/cm^2 .

2 Device design

2.1 Quantum structure design The nonlinear devices presented in this work consist of two major parts – the pump QCL active region and the giant nonlinearity. For pumping purposes we used injectorless QCL designs emitting at 7 μm similar to the one in [5]. Injectorless designs have the advantage of high gain [6], and thus low threshold current density which is important for good performance of the nonlinear device. The nonlinear structure was designed to have an enhanced nonlinear response at the pumping frequency.

The conduction band structure of quantum well based nonlinearity is shown in Fig. 1. The layer sequence (in nm) for this nonlinearity was as follows: 6/4.67/0.85/2.18. Here, the $\text{Al}_{0.6}\text{In}_{0.4}\text{As}$ barriers are shown in regular font and $\text{Ga}_{0.35}\text{In}_{0.65}\text{As}$ wells are underlined. The middle 2 nm of the thick barrier were doped with Si to $4 \times 10^{17} \text{cm}^{-3}$. The calculated energy spacings between levels 1-2 and 1-3 were 178 meV and 355 meV. The corresponding dipole matrix elements were calculated to be 1.51 nm, 1.84 nm and 0.57 nm for the 1-2, 2-3 and 3-1 transitions respectively.

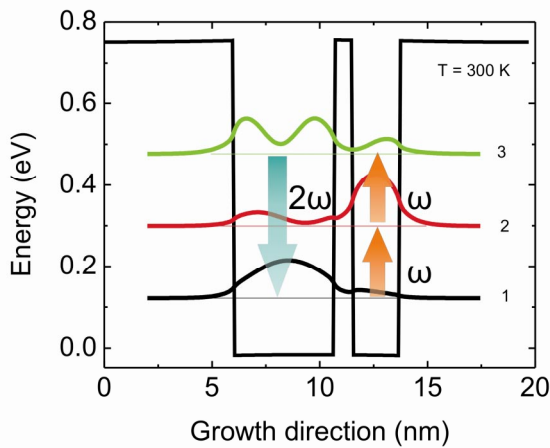


Figure 1 Conduction band diagram for the nonlinear structure, optimized for second-harmonic generation around 3.5 μm

It can be shown that such quantum well system has resonant nonlinear properties, and its second-order nonlinear susceptibility is given as [7]:

$$\chi^{(2)} = \frac{e^3 N z_{12} z_{23} z_{31}}{\epsilon_0 \hbar^2} \times \frac{1}{[(2\omega - \omega_{31}) + j\gamma_{31}][(\omega - \omega_{12}) + j\gamma_{12}]} \quad (1)$$

Here, N is the average carrier density in the structure, z_{ij} , ω_{ij} and $2\gamma_{ij}$ are the dipole matrix element, angular frequency and the transition linewidth FWHM corresponding to the intersubband transition between levels i and j . The nonlinear response as a function of pump frequency for nonlinearities designed for 3.5 μm and 2.7 μm SHG are shown in Fig. 2. The details for the 2.7 μm SHG structure can be found in [8]. In our calculations, we assumed the pump and the SH frequencies to be resonant with the corresponding intersubband transitions, and the transition linewidth FWHM were assumed equal to 16 meV. From Fig. 2 it can be clearly seen that the quadratic susceptibility can reach giant value – above 10^4 pm/V at resonance. This is several order of magnitude higher than for any nonlinear bulk material, such as GaAs, GaSe, etc. However, it should be noted, that experimentally it can be quite challenging to achieve it due to deviations in layer thicknesses, uncertainties in doping etc. Probably the biggest challenge lies in the correct prediction of the highest energy level, as it can be affected not only by the non-parabolic, but also non spherical dispersion of the band [4]. Therefore, multiband k.p. simulations are preferred, which should give higher accuracy. In our work, 8 band k.p. simulations were used for the band structure simulations of our nonlinear structures.

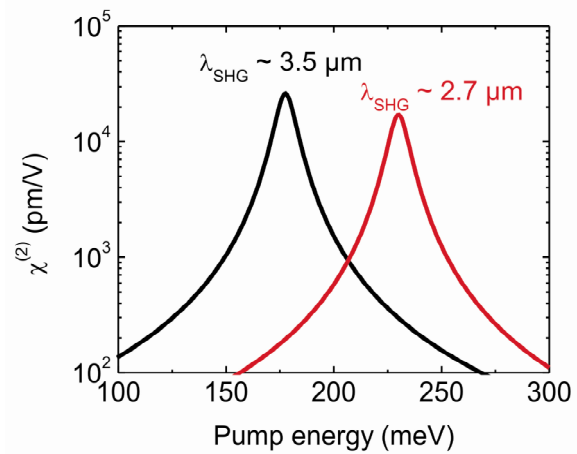


Figure 2 Resonant nonlinear response for two QW-based nonlinearities, optimized for SHG around 3.5 μm and 2.7 μm .

2.2 Device fabrication Quantum well based nonlinearities are extremely attractive not only because they possess giant nonlinear properties but also because they can be readily integrated with active quantum cascade lasers.

Our device growth started with the MBE growth of 60 repetitions of injectorless QCL active region, emitting around 7 μm , followed by 50 nm of InP etch-stop layer and 50 repetitions of the nonlinear structure shown in Fig. 1. Afterwards the top nonlinear layer was patterned into 50 % duty-cycle quasi-phase-matching gratings of different length by selective wet-chemical etching. Next, the sample was cleaned and transferred into the MOVPE chamber, where the top 4 μm of low-doped ($4 \cdot 10^{16} \text{ cm}^{-3}$) InP waveguide, 0.2 μm of high doped ($5 \cdot 10^{18} \text{ cm}^{-3}$) InP and 50 nm of GaInAs n^{++} contact layer were overgrown. The sample was then processed into conventional ridge waveguide devices by a combination of processing steps including, dry-etching, PECVD, e-beam evaporation of metals, and substrate thinning. Finally, the devices were soldered epi-side-up with Sn on copper heatsinks and wire bonded for characterisation. The schematic device picture is shown in Fig. 3. In simplest case, neglecting the pump depletion effects, and taking into account only the fundamental TM_{00} modes, the nonlinear power can be written as:

$$P_{2\omega} = \frac{\omega^2}{2n_{\omega}^2 n_{2\omega} \epsilon_0 c^3} \left| \frac{\chi^{(2)}}{\pi} \right| \frac{P_{\omega}^2}{A_{\text{eff}}} l_{\text{eff}}^2 \quad (2)$$

Here, ω is the pumping frequency, $n_{\omega, 2\omega}$ are the effective refractive indices for the fundamental and the SH modes. A_{eff} , l_{eff} are the effective area and length of interaction respectively. The first one is related to the modal overlap between the fundamental and the nonlinear waves [8], while the latter one is a function of modal loss and wavevector mismatch [8].

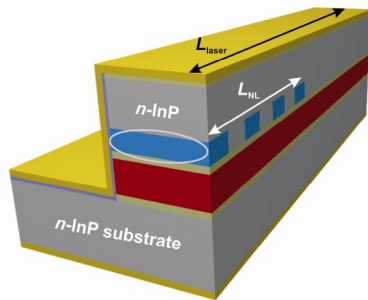


Figure 3 Schematic picture of a processed devices. From the longitudinal cross section view, the QPM grating close to the exit facet is visible.

3 Results and discussion For characterization, cleaved devices were characterized in the temperature range from 80 K to room-temperature in pulsed mode. A mounted laser bar consisted of 7 lasers with different QPM grating periods and a reference laser with the nonlinear layers etched away during processing. From simple 1D mode simulation, the wavevector mismatch between the fundamental and the SH TM_{00} modes was calculated to be around 1345 cm^{-1} . Thus, we expected the best performance from device with the QPM grating period close to $46 \mu\text{m}$. Experimentally, however, the best results were obtained for devices with QPM grating period of $57 \mu\text{m}$, corresponding to the wavevector mismatch of 1100 cm^{-1} . The results for this device are shown in Fig. 4-5. The discrepancy between the experiment and simulation might come from more complex interaction involving higher order transversal modes and parasitic phase-matching at an angle. These effects are currently under investigation and are expected to be reported elsewhere. Figure 4 shows light-output vs. current density (L - j) data at 80 K. The device was 3 mm long and $12 \mu\text{m}$ wide. The nonlinear QPM grating was 0.8 mm long with a period of $57 \mu\text{m}$. The facets were left uncoated. At low temperatures the device demonstrated $\sim 0.5 \text{ mW}$ SH power at a pumping power of 700 mW. As seen from Fig. 4, the SH power starts saturating at current densities above 3 kA/cm^2 . We attribute this to the power saturation effects and the appearance of higher order transversal modes, which suffer from poor modal overlap between the linear and nonlinear signals, thus leading to inefficient mixing. The power saturation effects are also expected to be present in our devices as due to the compact size of our device pump power levels of the order of hundred mW should be sufficient to saturate the optical transition between levels 1-2 in the nonlinear structure [8].

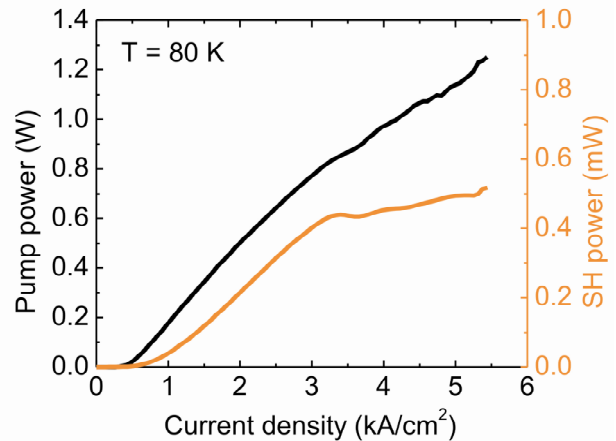


Figure 4 L - j data at $T = 80 \text{ K}$. The device was operated in pulsed mode with 500 ns long pulses at a repetition rate of 10 kHz. The SH output power was measured with a calibrated MCT detector, equipped with two short-wave pass filters..

It can be seen that current densities of operation are kept low – similar to ones for conventional mid-IR QCLs. This is a significant advantage over previous concepts of nonlinear QCL based devices [9, 10], which were operating at very high current densities and thus were limited to cryogenic operation. In our case, the device was lasing up to room-temperature (RT). RT L - j and spectral data are summarized in Fig.5.

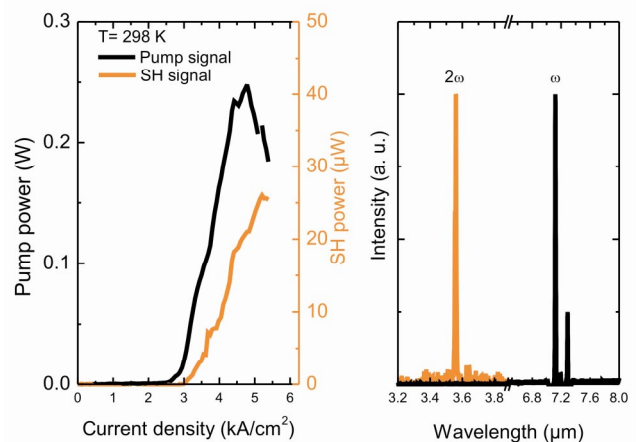


Figure 5 Room-temperature L - j (left) and spectral (right) data for the same device. For spectral measurements, the VERTEX 70 FTIR system was used. For SH spectral measurements, the detector was equipped with a short-pass filter to avoid any influence from the pump signal.

At room-temperature, the maximum second-harmonic output power is $\sim 30 \mu\text{W}$, which is one of the highest SH powers at this temperature, and wavelength reported so far [11]. The RT threshold current density is around 3 kA/cm^2 , which can be still lowered by reducing the average doping level in the pump active region.

The full potential of our approach is well illustrated by the demonstration of room-temperature emission at wavelengths $\sim 2.7 \mu\text{m}$ with threshold current densities as low as 1.5 kA/cm^2 . The results of the latter device have been recently published in more detail elsewhere [8]. Despite the achieved results, we believe that the device performance can be further improved. Mainly, by carefully optimizing the growth of the nonlinear structures, in order to get them resonant with the pump emission. Due to the resonant nature of the nonlinear properties, our structures are quite sensitive to relatively small deviations in composition and layer thicknesses. In the present devices we seem to be somewhat off-resonance as the additional loss due to resonant absorption in the nonlinear structure is negligible and the internal conversion efficiency is lower than estimated.

4 Conclusion We described the concept of short-wavelength quantum cascade laser source based on intracavity frequency doubling in monolithically integrated giant nonlinearity. Our reported devices successfully operated up to room-temperature at wavelengths $\sim 3.5 \mu\text{m}$. RT output of $30 \mu\text{W}$ for uncoated devices has been demonstrated. We believe that for fully optimized devices, SH powers exceeding mW level at room-temperature should be available in the entire wavelength range between $2.5 \mu\text{m}$ and $3.8 \mu\text{m}$. This, in turn, would lead to a possibility of extremely broadband tuneable single chip based device with the possibility of tuning the fundamental signal from $8 \mu\text{m}$ to $5 \mu\text{m}$, and in turn the second-harmonic signal signal from $4 \mu\text{m}$ to $2.5 \mu\text{m}$. This could be realized, for instance, in a similar way as with broadband tunable distributed feedback (DFB) QCLs [12]. Except in our case one could vary the QPM grating period, providing phase-matching for the desired wavelength.

Acknowledgements Walter Schottky Institut group gratefully acknowledges the financial support by the Excellence Cluster "Nanosystems Initiative Munich (NIM)" and the UT Austin group acknowledges the Texas Higher Education Coordinating Board "Norman Hackerman Advanced Research Program" award.

References

- [1] M. Razeghi, *IEEE J. Select. Top. Quantum Electron.* **15**, 941-950 (2009).
- [2] O. Cathabard, R. Teissier, J. Devenson, J. C. Moreno, and A. N. Baranov, *Appl. Phys. Lett.* **96**, 0141110 (2010).
- [3] S. Y. Zhang, D. G. Revin, J. W. Cockburn, K. Kennedy, A. B. Krysa, and M. Hopkinson, *Appl. Phys. Lett.* **94**, 031106 (2009).
- [4] Y.-H. Cho and A. Belyanin, *J. Appl. Phys.* **107**, 053116-1 – 053116-7 (2010).
- [5] S. Katz, G. Boehm, and M.-C. Amann, *Electron. Lett.* **44**, 580-581 (2008).
- [6] S. Katz, A. Vizbaras, G. Boehm, and M.-C. Amann, *Opt. Eng.* **49**, 111107 (2010).
- [7] R. W. Boyd, *Nonlinear Optics* (Academic Press, New York, 2008), pp. 69-204.
- [8] A. Vizbaras, M. Anders, S. Katz, C. Grasse, G. Boehm, R. Meyer, M. A. Belkin, and M.-C. Amann, *IEEE J. Quantum Electron.* **47**, 691-698 (2011).
- [9] C. Gmachl, A. Belyanin, D. L. Sivco, M. L. Peabody, N. Owschimikow, A. M. Seargent, F. Capasso, and A. Y. Cho, *IEEE J. Quantum Electron.* **30**, 1345-1355 (2003).
- [10] O. Malis, A. Belyanin, C. Gmachl, D. L. Sivco, M. L. Peabody, A. M. Seargent, and A. Y. Cho, *Appl. Phys. Lett.* **84**, 2721-2723 (2004).
- [11] M. Jang, R. W. Adams, J. X. Chen, W. O. Charles, C. Gmachl, L. W. Cheng, F.-S. Choa, and M. A. Belkin, *Appl. Phys. Lett.* **97**, 141103 (2010).
- [12] B. Lee, M. A. Belkin, R. Audet, J. MacArthur, L. Diehl, C. Pflügl, and F. Capasso, *Appl. Phys. Lett.* **91**, 231101 (2007).